Coexisting Fast-Scale and Slow-Scale Instability in Current-Mode Controlled DC/DC Converters: Analysis, Simulation and Experimental Results

Yanfeng Chen, Chi K. Tse, *Fellow, IEEE*, Shui-Sheng Qiu, Lars Lindenmüller, and Wolfgang Schwarz, *Member, IEEE*

***Abstract*—This paper investigates the coexisting fast-scale and slow-scale bifurcations in simple dc/dc converters under peak current-mode control operating in continuous conduction mode. Our focus is the boost converter as it is a representative form of dc/dc converter requiring current-mode control. Effects of varying the input voltage and some chosen parameters on the qualitative behavior of the system are studied in detail. Analysis based on a nonlinear simplified discrete-time model, which takes into account the effects of parasitics, is performed to investigate the coexistence of fast-scale and slow-scale bifurcations, and to identify the different types of bifurcation. Boundaries of stable region, slow-scale bifurcation region, fast-scale bifurcation region, coexisting fast and slow-scale bifurcation region are identified. Experimental measurements of the boost converter are provided for verification of the analytical results.**

***Index Terms*—Bifurcation, current-mode control, dc/dc converters, fast-scale instability, slow-scale instability.**

I. Introduction

THE current-mode control scheme is a widely used control method for dc/dc converters, especially for the boost and buck-boost types of dc/dc converters [1]. Bifurcation behaviors in dc/dc converters under current-mode control have been reported recently [2]–[5]. Generally, two distinct types of bifurcation have been identified for such circuits, namely slow-scale bifurcation and fast-scale bifurcation. The slow-scale bifurcation can be regarded as a kind of low-frequency instability which is caused by the voltage feedback loop permitting low-frequency oscillation [6]–[8]. The fast-scale bifurcation, which is caused by inner current loop instability, is often found in current-mode controlled converters, and it manifests as period-doubling in the time scale, as reported in Iu and Tse [9] for parallel boost converters, Wong and Tse [10] for noise-coupled boost converters, Iu *et al.* [11] and Wu *et al.* [12] for power-factor-correction converters, and Mazumder *et al.* [13] for voltage-mode buck converters with an input filter. The fast-scale and slow-scale bifurcations have been independently investigated as it has been generally believed that the outer voltage loop is much slower than the inner current loop and the two loops can be considered non-interacting. As a result, slow-scale bifurcation and fast-scale bifurcation have been studied separately. However, in practice, under certain conditions, slow-scale and fast-scale bifurcations can occur simultaneously, as shown in our earlier preliminary work [14].

Current-mode controlled dc/dc converters usually have two feedback loops: a current feedback loop and a voltage feedback loop. The latter provides the necessary current reference for the former. The outer voltage feedback loop contains typically a proportional-integral controller and hence has a low-pass characteristic, whereas the inner current loop is as fast as the switching frequency. The instability in the outer voltage loop is a slow-scale phenomenon, whereas the instability of the inner current loop is a fast-scale one which can also occur with the voltage feedback loop opened and is sometimes called "open-loop instability" [15]. It has been well known that the fast-scale instability is related to the value of the duty ratio d, and the range of stability can be increased by applying a compensation ramp. The instability for values of d outside a certain range is usually regarded as being associated with the current feedback loop as it occurs with the voltage feedback opened. Moreover, the two loops actually affect each other as the current reference used to program the inductor current in the inner current loop is provided by the outer voltage loop. Therefore, the two mechanisms responsible for the fast-scale and slow-scale bifurcations can actually interact with each other, leading to possible coexisting fast-scale and slow-scale bifurcations, and the stable range of d should address the overall instability of the system, rather than either the fast-scale or slow-scale instability. However, up to now, the stability analysis reported stops short of putting such interaction into proper consideration.

In general, the rising slope of the inductor current and the compensation slope are the main parameters affecting fast-scale bifurcation, whereas the feedback gain g and time constant τ_a are responsible for slow-scale bifurcation. In our earlier study [14], we have observed that the current-mode controlled boost converter can exhibit coexisting fast-scale and slow-scale bifurcations under variation of these parameters. In practice, the two important design parameters, i.e., input voltage and load resistance, may vary during operation. The other parameters such

Manuscript received July 4, 2007; revised October 30, 2007. Current version published November 21, 2008. This project was supported by Hong Kong Polytechnic University under Grant G-U284. This paper was recommended by Associate Editor S. Banerjee.

Y. Chen was with the Department of Electronic and Information Engineering, Hong Kong Polytechnic University, Hunghom, Kowloon, Hong Kong. He is now with the College of Electronic and Information Engineering, South China University of Technology, Guangzhou, China.

C. K. Tse is with the Department of Electronic and Information Engineering, Hong Kong Polytechnic University, Hunghom, Hong Kong (e-mail: encktse@polyu.edu.hk).

S.-S. Qiu is with the College of Electronic and Information Engineering, South China University of Technology, Guangzhou, China.

L. Lindenmüller and W. Schwarz are with the Technical University of Dresden, Dresden, Germany.

Digital Object Identifier 10.1109/TCSI.2008.923282

as inductance, capacitance and reference voltage are generally fixed by design and are not assumed to be varying. The converters may undergo bifurcations during operation depending on various combinations of the continuously varying parameters. Furthermore, the input voltage is one of the factors that affect both the rising and falling slopes of the inductor current and hence the duty ratio. It can thus be expected that variation of the input voltage will affect both the fast-scale and slow-scale instabilities of the system. The load resistance also plays a role in determining the occurrence of bifurcation as it directly affects the natural frequency of the converter circuit, which may interact with the switching frequency to generate quasi-periodic behavior, as studied in Aroudi *et al.* [6]. It is therefore of particular importance to study the bifurcation patterns over the parameter space of input voltage, load, feedback gain and feedback time constant, and to identify the boundaries of stable region, slow-scale bifurcation region, fast-scale bifurcation region, and the coexisting region. Such information will help designers determine the safe nominal operating point and the amount of clearance from instability.

DC/DC converters may operate in continuous conduction mode (CCM) or discontinuous conduction mode (DCM), depending upon the parameter choice and the dynamical status. It is possible that a dc/dc converter toggles between the two operating modes in a rather complex manner. In our study in this paper, the converter parameters are chosen so that CCM is the default operating mode. Thus, *normal stable operation* refers to stable period-1 operation in CCM. Subsequently, *instability* refers to operation that is *not* the normal stable operation, and *bifurcation* refers to the change from one type of operation to another.

In general, analysis methods for dc/dc converters can be based on: 1) continuous-time models; 2) discrete-time models; or 3) combination of continuous-time and discrete-time models. It is known that small-signal analysis methods based on state-space averaged continuous-time models fail to study fast-scale dynamics, whereas exact discrete-time modeling techniques capture both fast-scale dynamics and slow-scale dynamics [2], [13]. Discrete-time modeling methods have been applied to study the interacting effects of the two loops in the closed-loop current-mode controlled boost converter [14], in which the state variables of power stage circuit and voltage feedback network are integrated in the model. By truncating the transition matrix series [16], a simplified discrete-time model can be derived [14], which can be regarded as an averaged discrete-time model. It is worth mentioning here that the explicit simplified model can be particularly useful in reducing the computational load, and in explaining dependance of the interacting instability on parameters of the system, since the analytical expressions for equilibrium points and solutions of characteristic polynomial can be obtained readily.

This paper is organized as follows. In Section II, we will review the operation of dc/dc converters under peak-current-mode (PCM) control. In Section III, we will present some typical waveforms for current-mode controlled boost, buck and buck-boost converters under normal stable operation, slow-scale bifurcation, fast-scale bifurcation, coexisting fast-scale and slow-scale bifurcation, and "saturated" operation (in which the duty cycle saturates to a maximum or minimum value limited by the current-mode controlled IC as the error amplifier in the voltage feedback loop saturates). The corresponding typical waveforms for the boost converter are confirmed by experimental measurements in Sections IV and VI. Analysis of these bifurcation phenomena using a simplified discrete-time model will be presented in Section V, which is based on tracking the movements of the eigenvalues of the Jacobians evaluated at the appropriate operating states [17]. In Section VI, we will present the boundaries in the parameter space of input voltage, load resistance, feedback gain, and time constant by "exact" cycle-by-cycle simulations of the actual system and experimental results, and will compare them with those obtained by the analytical method derived in Section V. Here, the load resistance, feedback gain and time constant in the outer voltage loop are selected as the parameters for slow-scale bifurcation, whereas the input voltage is selected as the parameter for both the fast-scale and slow-scale bifurcation. Finally, we conclude this paper in Section VII.

II. Operation of the Current-Mode Controlled Converter

The closed-loop current-mode controlled boost, buck and buck-boost converters are shown in Fig. 1(a)–(c), respectively. The waveforms of the control voltage and the inductor current analog are illustrated in Fig. 1(d). Each system has an outer voltage loop and an inner current loop. The voltage loop consists of an error amplifier (EA) and a proportional-integral controller, the output of which provides the reference for the inner current loop. The inner current loop consists of a current transformer and a current sensing amplifier (IA). A compensation ramp is added to stabilize the converter if a wide range of output voltage is required [8]. The output of the current loop is then connected to the inputs of the comparator whose output is used to reset a flip-flop latch to give a pulse-width modulated waveform to control switch S_T. The operation can be briefly described as follows. The flip-flop latch is set periodically by the clock signal, turning on the switch S_T. Then, if the inductance L is large enough, the inductor current i_L goes up linearly, and is compared with a reference level, which is equal to the output of the error amplifier of the voltage loop minus the compensation ramp signal. When the peak inductor current reaches the reference level, the output of the comparator resets the flip-flop, thereby turning off the switch. When the switch is off, the inductor current falls almost linearly if the output capacitor is sufficiently large too. The cycle repeats when the flip-flop is set again by the clock. Typical waveforms of the converter operating in CCM are shown in Fig. 1(d), where m_c is the slope of the compensation ramp signal, M is the sampling gain of the inductor current, and m_1 and m_2 are the rising and falling slopes of the inductor current with the switch on and off, respectively.

III. A Glimpse at Bifurcation Behavior From Simulations

We begin with a series of typical waveforms which have been obtained from exact cycle-by-cycle computer simulations. The purpose is to provide a quick preview of the kinds of phenomena that would occur in the current-mode controlled boost and buck-boost converters under variation of the input voltage and load resistance, and also in the buck converter under variation of

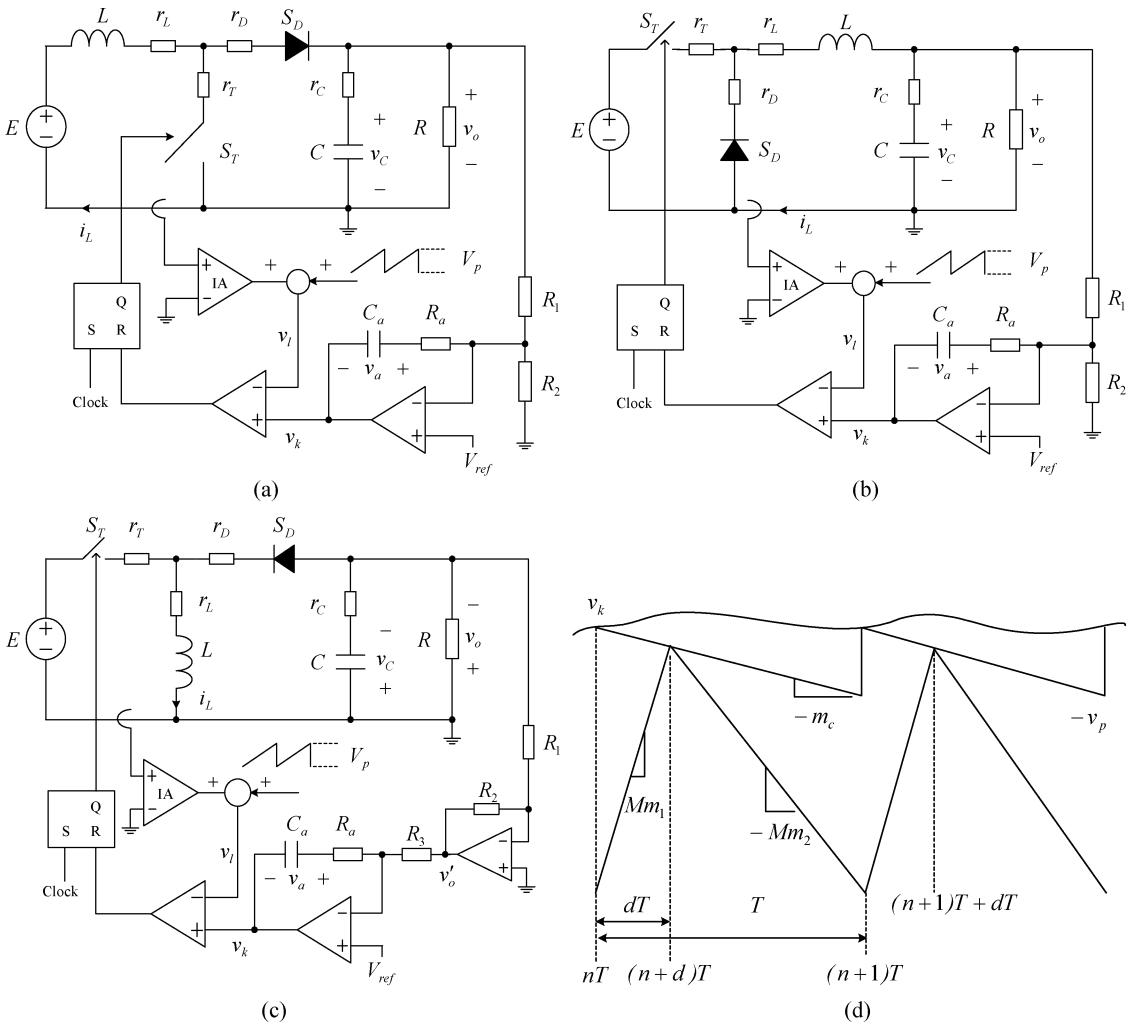

Fig. 1. Basic dc/dc converters under current-mode control and typical waveforms. (a) Boost converter. (b) Buck converter. (c) Buck-boost converter. (d) Typical waveforms of the control voltage v_k and the inductor current analog.

the compensation slope. For consistency with the usual practice, we have limited the value of the duty cycle between 0.1 and 0.9. We will omit the cases of stable, fast-scale and "saturated" operations as they have been well documented elsewhere [2]. Our focus in this paper is the coexistence of fast-scale and slow-scale bifurcations. Moreover, the unstable operations associated with "saturation" of control signals (typically manifested as saturation of the duty cycle) will not be examined because these operations occur well beyond the boundaries of the first fast-scale or slow-scale bifurcations.[1] The main parameters affecting fast-scale bifurcations are the rising slope of the inductor current m_1, and the compensation slope m_c, whereas those affecting slow-scale bifurcations are the voltage feedback gain g and time constant τ_a. In our earlier work [14], normal periodic operation, slow-scale bifurcation, fast-scale bifurcation, coexisting fast-scale and slow-scale bifurcation, and "saturated" operation (border collision) have been observed, and it has been shown that slow-scale bifurcation can be eliminated by increasing the feedback gain or time constant, while fast-scale bifurcation can be eliminated by increasing m_c, or decreasing m_1 via increasing L. Here, we will look at the complex behavior in more detail when the input voltage E or load resistance R are changed. To facilitate simulation study, we choose parameter values as listed in Table I. Typical waveforms are shown in Figs. 2–4. Here, we fix $L = 165$ μH and $m_c = 11.125 \times 10^3$ A/s. Similar scenarios can be observed when R, g and τ_a are changed. We omit the waveforms here as they are similar to those shown in Figs. 2–4.

[1]By "first" fast-scale or slow-scale bifurcations we mean those bifurcations adjacent to the normal operation. Such bifurcations are the only practically meaningful types of bifurcation as they correspond to the mechanisms through which the system loses stability.

IV. Experimental Observation

For the experimental study, we focus on the boost converter, as it is the most common type of converters to employ current-mode control. The experimental schematic circuit for the current-mode controlled boost converter is shown in Fig. 5, where the control IC is a low-power BiCMOS current-mode PWM control IC UCC3802. The reference voltage of UCC3802 is DC 5 V, which is divided internally to 2.5 V and serves as the reference voltage of the error amplifier, as shown in Fig. 1(a).

As our intention is to probe into coexisting bifurcation, the time constant of the voltage feedback loop is chosen to be relatively small in order to limit the bandwidth of the feedback

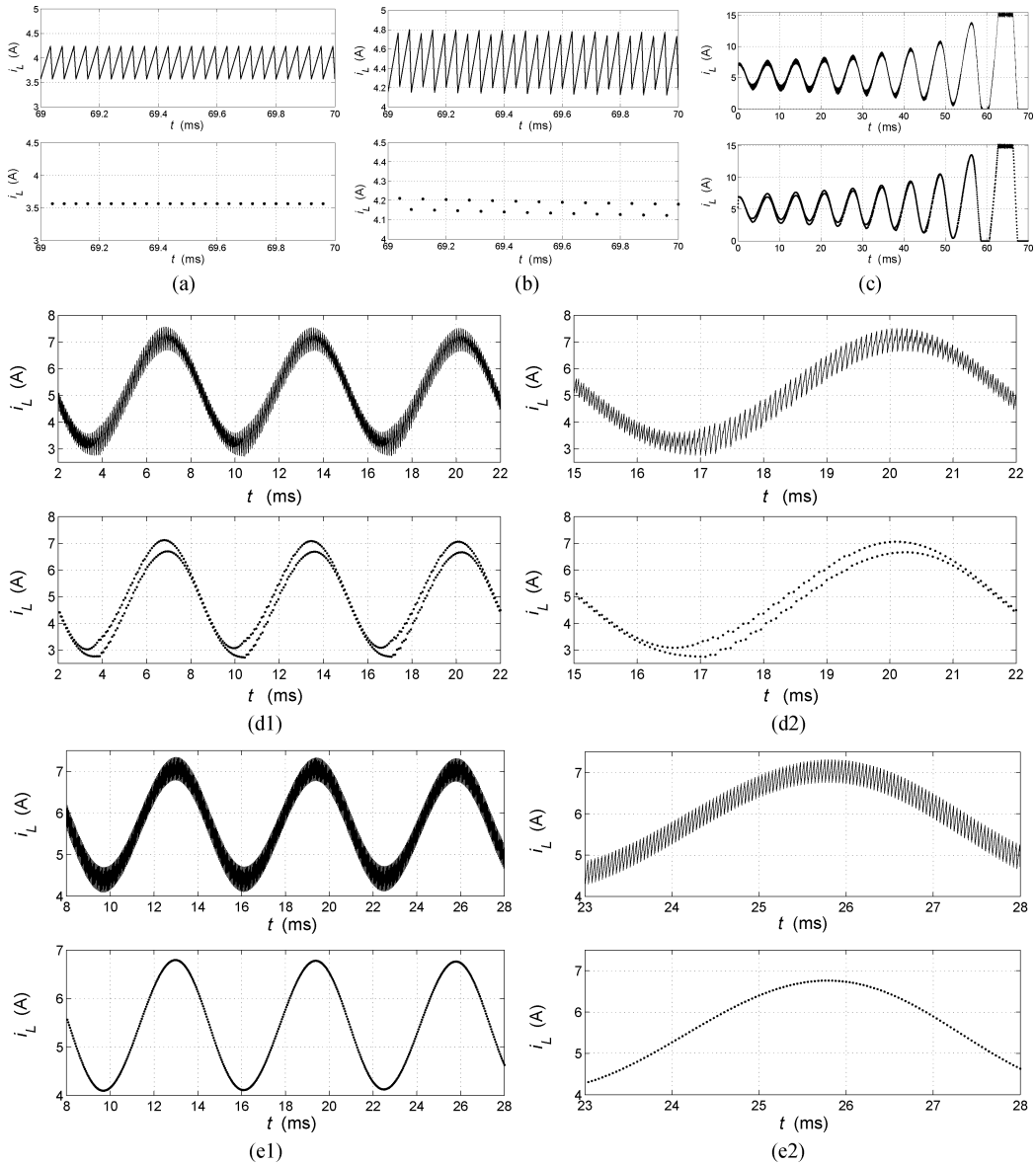

Fig. 2. Simulated waveforms for the current-mode controlled boost converter under different input voltages with $L = 165\ \mu$H, $\tau_a = 0.3196\ hboxms$, $g = 1.0$ and $m_c = 11.125 \times 10^3$ A/s. (a)–(d) are with $R = 30\ \Omega$, and (e) is with $R = 25\ \Omega$. Upper trace: actual waveforms, lower trace: sampled-data waveforms collected at $t = nT$. (a) Stable periodic operation with $E = 3.70$ V; (b) fast-scale bifurcation with $E = 3.40$ V; (c) saturated operation with $E = 3.0$ V; (d1)–(d2) coexisting fast-scale and slow-scale bifurcation with $E = 3.04$ V: (d1) time-domain waveforms of inductance current i_L and (d2) close-up view of (d1); (e1)–(e2) slow-scale bifurcation with $E = 3.28$ V: (e1) time-domain waveforms of i_L; (e2) close-up view of (e1).

network. Then, the load or the input voltage is changed. Typical waveforms are shown in Fig. 6, which agree very well with the simulation results shown earlier in Fig. 2. Note that the amplitude of the inductor current here is ten-fold larger than that shown in Fig. 6. This is because the inductor current sampling gain in the experimental circuit is 0.1, and an upper limit of 10 A has been imposed on the inductor current which causes the saturation of the waveform, as shown in Fig. 6(c).

V. Bifurcation Analysis of the Closed-Loop Current-Mode Controlled Converter

From the foregoing simulation studies and experimental results, we have briefly observed slow-scale bifurcation, fast-scale bifurcation and coexisting bifurcation in certain parameter ranges. In this section we will analyze these bifurcations by using a suitable model. We will take the boost converter as an example and derive a simplified discrete-time model that describes the dynamics of the system by implementing some appropriate approximations on the exact discrete-time model [14], [18], and investigate the dynamical behavior by examining the movements of the characteristic multipliers (eigenvalues) of the Jacobians as some chosen parameters are varied [17], [19]. The analysis method for the boost converter can be easily extended to buck and buck-boost converters.

Our analysis in this paper first assumes that the inductor and output capacitor are sufficiently large that the inductor current and output voltage have linear waveform segments. Moreover, we may also take into account the effects of parasitics, e.g., by modeling the power switches and circuit elements by their ideal

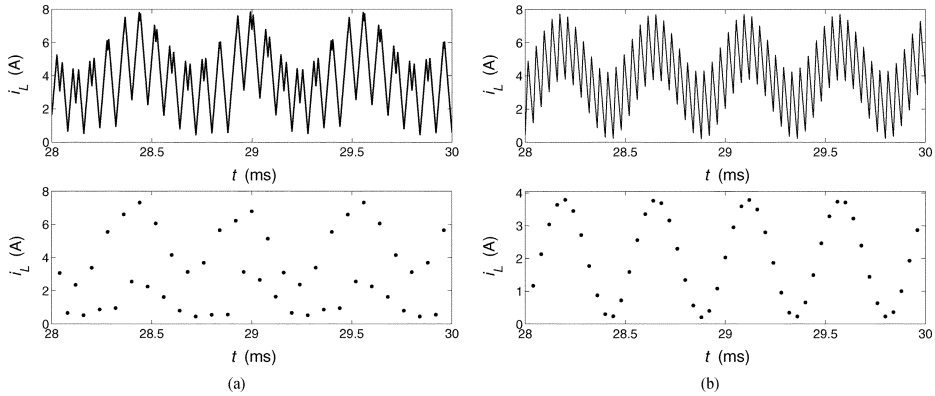

Fig. 3. Simulated waveforms for current-mode controlled buck converter showing coexisting bifurcation and slow-scale bifurcation. $D = 0.5$, $R = 1.5\ \Omega$, $g = 0.2$ and $\tau_a = 0.01254$ ms. (a) Coexisting bifurcation at compensation slope $m_c = 0$; (b) slow-scale bifurcation with $m_c = 6.25 \times 10^3$ A/s.

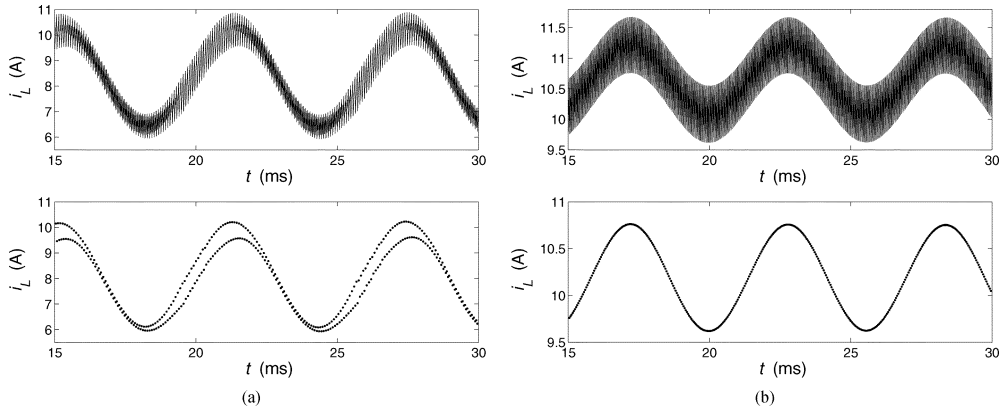

Fig. 4. Simulated waveforms for current-mode controlled buck-boost converter showing interacting bifurcation and slow-scale bifurcation. $m_c = 12.5 \times 10^3$ A/s, $g = 1.0$ and $\tau_a = 0.3162$ ms. (a) Coexisting bifurcation with $E = 4.590$ V and $R = 15\ \Omega$; (b) slow-scale bifurcation with $E = 5.615$ V and $R = 10\ \Omega$.

TABLE I
CIRCUIT PARAMETERS FOR SIMULATION STUDY

Component/parameter	Value for Boost	Value for Buck	Value for Buck-boost
Input voltage E	2.5–18 V	30 V	2.5–40 V
Inductance L	165 μH	165 μH	165 μH
Parasitic resistance L, r_L	40 mΩ	40 mΩ	40 mΩ
Capacitance C	1500 μF	1500μF	1500 μF
Parasitic resistance C, r_C	30 mΩ	30 mΩ	30 mΩ
Parasitic resistance of transistor, r_T	55 mΩ	55 mΩ	55 mΩ
Parasitic resistance of diode, r_D	10 mΩ	10 mΩ	10 mΩ
Load resistance R	15 – 50 Ω	1.5 Ω	15 – 50 Ω
Switching frequency f_s	25 kHz	25 kHz	25 kHz
Reference output voltage $V_{\rm ref}$	2.5 V	0.75 V	2.5 V
Voltage divider R_1, R_2	47 kΩ, 6.8 kΩ	47.5 kΩ, 2.5 kΩ	53.6 kΩ, 6.8 kΩ
Resistance R_3	NA	NA	5.9 kΩ
Control network R_a, C_a	10–100 kΩ, 2.2–22 nF	10–100 kΩ, 2.2–22 nF	10–100 kΩ, 2.2–22 nF
Compensation ramp V_p	0.445 V	0–0.5 V	0.50 V
Inductance current sampling gain M	0.3 V/A	0.1 V/A	0.3 V/A

models in series with parasitic resistances. In general, these parasitics do not affect the qualitative results regarding the bifurcation patterns but are found to shift the critical points at which bifurcation occurs, as observed previously by Banerjee and Chakrabarty [4].

A. Derivation of State Equations

The simple dc/dc converters described above can be regarded as systems with a variable structure that toggles their topologies according to the states of the switches. Typically, when operating in CCM, two switch states can be identified.

$$\text{State } 1: \text{switch } S_T \text{ on and diode } S_D \text{ off.}$$
$$\text{State } 2: \text{switch } S_T \text{ off and } \textit{diode}\ S_D \text{ on.}$$

The two switch states toggle periodically in the steady state. We assume that the circuit takes state 1 for $nT_s \le t < (n + d)T_s$, and state 2 for $(n + d)T_s \le t < (n + 1)T_s$, where n is an integer, T_s is the switching period, and d is the duty cycle,

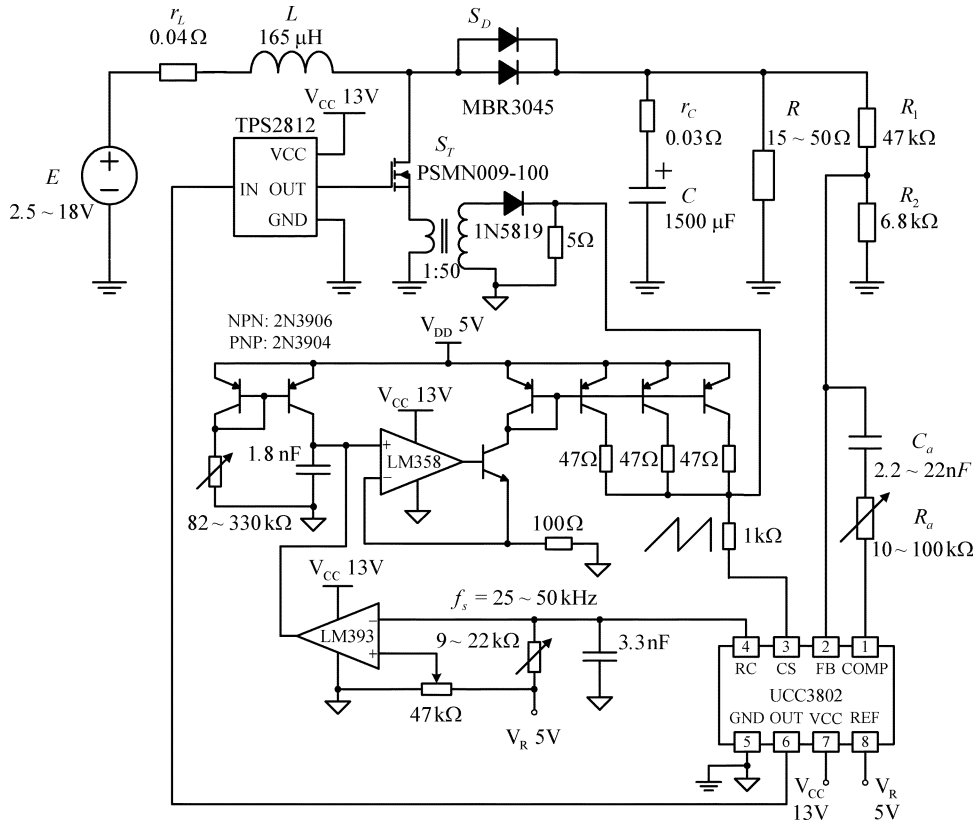

Fig. 5. Schematic diagram of experimental boost converter under current-mode control.

which is defined as the ratio of the turn-on time of switch S_T to the switching period T_s. In a closed-loop converter system, d is usually a function of the system's state variables, as will be discussed in a later section.

As shown in Fig. 1(a), the compensator used here is a first-order PI controller. In addition to the two state variables chosen from the converter (i.e., inductor current i_L and output capacitor voltage v_C), the voltage across the compensation capacitor, v_a, can be described by the following state equation:

$$\frac{dv_a}{dt} = g\left(\frac{v_o}{\tau_a} - \frac{k_d V_{\text{ref}}}{\tau_a}\right) \tag{1}$$

where $v_o = v_C/(1+k_c)$ is the output voltage of the system for state 1, V_{ref} is the reference output voltage, $k_d = (R_1 + R_2)/R_2$ is the ratio of the voltage divider, and $g = R_a/R_1$ and $\tau_a = R_aC_a$ denote the DC gain and time constant of the voltage feedback network, respectively. Here, k_c is defined as $k_c = r_C/R$. The system is thus third-order, with the possible choice of state vector as

$$\mathbf{x} = \begin{bmatrix} i_L & v_C & v_a \end{bmatrix}^T \tag{2}$$

where superscript T denotes matrix transposition. Thus, the control signal, v_k, can be expressed as a linear function of the system's state vector $\mathbf{x}$, i.e.,

$$v_k = k_0 + \mathbf{k_1}\mathbf{x} \tag{3}$$

where $k_0 = V_{\text{ref}}(1+gk_d)$, and $\mathbf{k_1}$ can be expressed as $\mathbf{k_1} = [0 - g/(1+k_c) - 1]$. Note that we only need to consider the expression of control signal v_k during state 1.

The system operating in CCM can be described by the following state equations:

$$\begin{aligned} \dot{\mathbf{x}} &= \mathbf{A}_1\mathbf{x} + \mathbf{B}_1 E \qquad \text{for } nT_s \le t < (n+d)T_s \\ \dot{\mathbf{x}} &= \mathbf{A}_2\mathbf{x} + \mathbf{B}_2 E \qquad \text{for } (n+d)T_s \le t < (n+d)T_s \end{aligned} \tag{4}$$

where E is the input voltage, and matrices $\mathbf{A}$'s and $\mathbf{B}$'s for the current-mode controlled boost converter are given as follows:

$$\mathbf{A}_1 = \begin{bmatrix} -\frac{r_L + r_T}{L} & 0 & 0 \\ 0 & -\frac{1}{\tau_m(1+k_c)} & 0 \\ 0 & \frac{g}{\tau_a(1+k_c)} & 0 \end{bmatrix} \tag{5}$$

$$\mathbf{A}_2 = \begin{bmatrix} -\frac{r_L + r_D}{L} - \frac{r_C}{L(1+k_c)} & -\frac{1}{L(1+k_c)} & 0 \\ \frac{1}{C(1+k_c)} & -\frac{1}{\tau_m(1+k_c)} & 0 \\ \frac{gr_c}{\tau_a(1+k_c)} & \frac{g}{\tau_a(1+k_c)} & 0 \end{bmatrix} \tag{6}$$

$$\mathbf{B}_1 = \mathbf{B}_2 = \begin{bmatrix} \frac{1}{L} \\ 0 \\ -\frac{gk_dV_{\text{ref}}}{\tau_a E} \end{bmatrix} \tag{7}$$

where $\tau_m = RC$. The corresponding expressions for current mode-controlled buck and buck-boost converters are given in Appendix I.

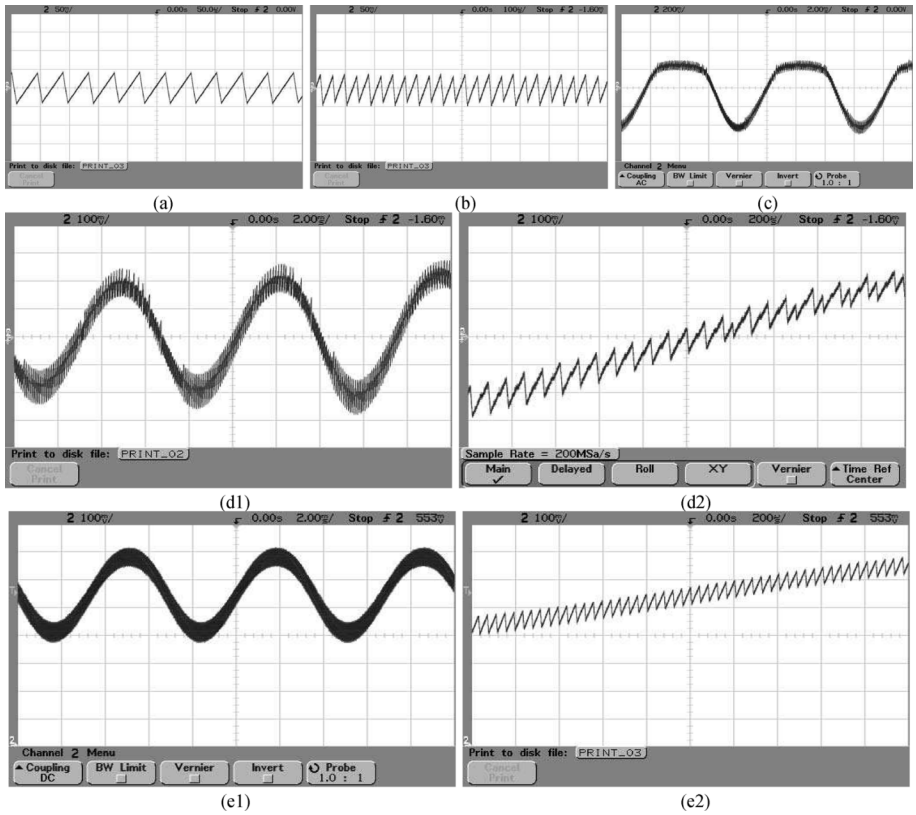

Fig. 6. Experimental results for current-mode controlled boost converter under different values of input voltage and load with $L = 165\ \mu$H, $\tau_a = 0.3196\ hboxms$, $g = 1.0$ and $m_c = 11.125 \times 10^3$ A/s. For (a)–(d), $R = 30\ \Omega$, and for (e), $R = 25\ \Omega$. (a) Stable periodic operation with $E = 3.900$ V; (b) fast-scale bifurcation with $E = 3.463$ V; (c) saturated operation with $E = 2.915$ V; (d1)–(d2) coexisting fast and slow-scale bifurcation with $E = 2.990$ V: (d1) time-domain waveforms of inductance current i_L and (d2) close-up view of (d1); (e1)–(e2) slow-scale bifurcation with $E = 3.239$ V: (e1) time-domain waveforms of i_L and (e2) close-up view of (e1).

B. Derivation of Simplified Discrete-Time Model

In this subsection, we attempt to derive a discrete-time map that describes the dynamics of the current-mode controlled converter system with a PI controlled voltage feedback loop, as shown in Fig. 1. The form of the discrete-time map we aim to get is

$$\mathbf{x}_{n+1} = \mathbf{f}(\mathbf{x}_n) \tag{8}$$

where subscript n denotes the value at the beginning of the nth cycle, i.e., $\mathbf{x}_n = \mathbf{x}(nT)$, and d_n represents the duty cycle during switching period. Note that for the closed-loop system, d_n should not appear explicitly in the state equation because it is related to $\mathbf{x}_n$ via a feedback function.

As mentioned above, the state equation for the circuit in any switch state can be written in the form of a linear differential equation, i.e., $\dot{\mathbf{x}} = \mathbf{A}_j\mathbf{x} + \mathbf{B}_j E$, where $j = 1, 2$. At the sampling instant, i.e., $t = nT_s$, switch S_T is turned on and the system enters state 1. At $t = t_s = (n + d_n)T_s$, S_T is turned off, and the system goes to state 2.

For the dc/dc converter operating in CCM, the input voltage E is supposed to be constant during the whole switching period. A nonlinear discrete-time model in the form of a stroboscopic map which relates the state variables $\mathbf{x}_n$ at instant nT to $\mathbf{x}_{n+1}$ at instant $(n+1)T$ can be written as follows:

$$\mathbf{x}_{n+1} = \mathbf{\Phi}_2\left((1-d_n)T_s\right)\left[\mathbf{\Phi}_1(d_nT_s)\mathbf{x}_n + \mathbf{\Psi}_1(d_nT_s)E\right] + \mathbf{\Psi}_2\left((1-d_n)T_s\right)E \tag{9}$$

where $\mathbf{\Phi}_j(\xi)$ and $\mathbf{\Psi}_j(\xi)$ are the corresponding system matrices given by

$$\mathbf{\Phi}_j(\xi) = e^{\mathbf{A}_j\xi} = \mathbf{1} + \sum_{k=1}^{\infty}\frac{1}{k!}\mathbf{A}_j^k\xi^k, \quad \text{for } j = 1, 2. \tag{10}$$

$$\mathbf{\Psi}_j(\xi) = \int_0^{\xi}\mathbf{\Phi}_j(\tau)\mathbf{B}_j\,d\tau, \quad \text{for } j = 1, 2. \tag{11}$$

To complete the derivation, we have to find the feedback relation that connects the duty cycle d_n and the state variables $\mathbf{x}_n$. Suppose v_l is the sensed inductor current analog, i.e., $v_l = Mi_L$, where M is the current sampling gain. During state 1, i_L rises linearly, and so does v_l. When v_l reaches the control signal level, switch S_T is turned off. According to the typical waveforms in Fig. 1(d), we may define a function $s(\mathbf{x}_n, d_n)$ as

$$s(x_n, d_n) = v_k(t_s) - v_l(t_s) - m_c d_n T_s, \tag{12}$$

where $v_l(t_s) = Mi_L(t_s) = M(i_{Ln} + m_1 d_n T_s)$, and v_k is a linear function of $\mathbf{x}$, as shown in (3).

Obviously, at $t = t_s$, we have $s(\mathbf{x}_n, d_n) = 0$, and S_T is turned off. In other words, $s(.) = 0$ defines the condition for the system to go from state 1 to state 2. Substituting (3) and $\mathbf{x}(t_s)$ in (12), and supposing $s(\mathbf{x}_n, d_n) = 0$, we get the duty-cycle d_n for the closed-loop current-mode controlled converter, which is determined by

$$d_n = \frac{k_0 + (\mathbf{k_1}\mathbf{\Phi}_1(d_nT_s) + \mathbf{k_2})\,\mathbf{x}_n + \mathbf{k_1}\mathbf{\Psi}_1(d_nT_s)E}{(Mm_1 + m_c)T_s} \tag{13}$$

TABLE II
EIGENVALUES FOR DIFFERENT VALUES OF INPUT VOLTAGE E FOR CURRENT-MODE CONTROLLED BOOST CONVERTER WITH $R = 30\ \Omega$, $\tau_a = 0.3196\ hboxms$ AND $g = 1.0$.

E (ms)	Eigenvalues	Modulus (complex pair)	Remarks
2.7968	1.0017± j0.034564, −1.1174	1.0022	duty cycle saturated (border collision)
2.8740	1.0009± j0.035694 , −1.1052	1.0015	duty cycle saturated (border collision)
2.9897	0.9999± j0.037216, −1.0860	1.0006	duty cycle saturated (border collision)
3.0669	**0.99929± j0.038142, −1.10727**	**1.0000**	**coexisting bifurcation**
3.1826	0.99843± j0.039426, −1.0524	0.99921	fast-scale bifurcation
3.2984	0.99765± j0.040609, −1.0318	0.99848	fast-scale bifurcation
3.3703	0.99719± j0.041303, −1.0189	0.99805	fast-scale bifurcation
3.4755	**0.99655± j0.042270, −1.0000**	**0.99745**	**fast-scale bifurcation**
3.5720	0.99600± j0.043113, −0.98273	0.99693	stable (normal period-1 orbit)
3.6957	0.99551± j0.043848, −0.96706	0.99648	stable (normal period-1 orbit)
3.8000	0.99477± j0.044971, −0.94214	0.99579	stable (normal period-1 orbit)

TABLE III
EIGENVALUES FOR DIFFERENT VALUES OF INPUT VOLTAGE E FOR CURRENT-MODE CONTROLLED BOOST CONVERTER WITH $R = 25\ \Omega$, $\tau_a = 0.3196\ hboxms$ AND $g = 1.0$.

E (ms)	Eigenvalues	Modulus (complex pair)	Remarks
3.036	1.0002± j0.036068, −1.0320	1.0027	duty cycle saturated (border collision)
3.1381	1.0001± j0.037522, −1.0178	1.0017	duty cycle saturated (border collision)
3.2062	1.0004± j0.038404, −1.0078	1.0011	duty cycle saturated (border collision)
3.2742	0.99979± j0.039231, −0.99754	1.0006	duty cycle saturated (border collision)
3.3423	**0.99924± j0.04001, −0.98702**	**1.0000**	**slow-scale bifurcation**
3.4444	0.99847± j0.041105, −0.97090	0.99931	stable (normal period-1 orbit)
3.5465	0.99775± j0.042127, −0.95451	0.99864	stable (normal period-1 orbit)
3.6486	0.99707± j0.043087, −0.93795	0.99800	stable (normal period-1 orbit)
3.7507	0.99643± j0.043997, −0.92130	0.99740	stable (normal period-1 orbit)
3.8527	0.99582± j0.044682, −0.90464	0.98683	stable (normal period-1 orbit)
3.9548	0.99524± j0.045690, −0.88800	0.99629	stable (normal period-1 orbit)

where k_0 and $\mathbf{k_1}$ are as defined earlier, $\mathbf{k_2} = [-\mathbf{M}\ \mathbf{0}\ \mathbf{0}]$, and $m_1 = E/L$ is the rising slope of the inductor current.

Expressions (9) and (13) define the exact discrete-time model of the system, which are transcendental and can only be solved numerically. By using the linear-ripple approximation $e^{\mathbf{A}t} \approx \mathbf{1} + \mathbf{A}t$, (9) and (13) can be simplified as

$$\mathbf{x}_{n+1} = [\mathbf{1} + T_s(d_n\mathbf{A}_1 + (1-d_n)\mathbf{A}_2)]\,\mathbf{x}_n + (d_n\mathbf{B}_1 + (1-d_n)\mathbf{B}_2)T_sE \quad (14)$$

$$d_n = \frac{k_0 + \mathbf{k}\mathbf{x}_n}{T_s\left[(Mm_1 + m_c) - \mathbf{k_1}(\mathbf{A}_1\mathbf{x}_n + \mathbf{B}_1E)\right]} \quad (15)$$

where $\mathbf{k} = \mathbf{k_1} + \mathbf{k_2} = [-M - g/(1+k_c) - 1]$. Obviously, (14) and (15) define a large-signal discrete-time average model of the system which is obtained under linear-ripple approximation. Under this approximation, the function $s(x_n, d_n)$ can be written as

$$s(x_n, d_n) = k_0 + \mathbf{k}\mathbf{x}_n - T_s\left[(Mm_1 + m_c) - \mathbf{k_1}(\mathbf{A}_1\mathbf{x}_n + \mathbf{B}_1E)\right]d_n \quad (16)$$

and $s(.) = 0$ defines the condition for the system to go from state 1 to state 2.

C. Equilibrium Points

Analysis of a nonlinear system usually begins with finding the equilibrium point $\mathbf{X}_Q$ and the corresponding duty cycle D_Q of the system, i.e., the steady-state solution. For the exact discrete-time model, as the expression of duty cycle is transcendental, numerical procedures have to be used for finding $\mathbf{X}_Q$. Yet for the simplified discrete-time model defined in Section V-B, the desired steady-state solution of state variables and duty cycle can be found by enforcing periodicity, i.e., putting $\mathbf{x}_{n+1} = \mathbf{x}_n = \mathbf{X}_Q$ and $d_n = D_Q$ in (14) and (15). In the steady state, the DC voltage across the output capacitor equals the system's output, i.e., $V_C = V_o$. Let $\mathbf{X}_Q = [I_L\ V_o\ V_A]^T$. Combining (14) and (15), and limiting solutions within practical ranges, $\mathbf{X}_Q$ and D_Q can be solved. For the current-mode controlled boost converter, we have

$$\begin{aligned} D_Q &= 1 - \frac{b + \sqrt{b^2 - 4c}}{2} \\ V_o &= k_d V_{\text{ref}} \\ I_L &= \frac{V_o}{R(1-D_Q)} \\ V_A &= V_{\text{ref}} - MI_L - \left(Mm_1 + m_c - \frac{gV_o}{\tau_m}\right)D_QT_s \end{aligned} \quad (17)$$

where $b = -(1+k_c)\left[E/V_O + (r_T - r_D)/R - rc/(R+rc)\right]$ and $c = (1+k_c)((r_T + r_L)/R)$. Similar expressions for the buck and buck–boost converters under current-mode control are shown in Appendix I.

D. Derivation of the Jacobian of the Simplified Discrete-Time Model

In this section, we aim to find the Jacobian for any given equilibrium state. The essence of using a Jacobian in the analysis of dynamical systems lies in the capture of the dynamics in a small neighborhood of the equilibrium point or orbit. Then, by inspecting the eigenvalues of the Jacobian, we are able to determine the stability of the equilibrium state. Furthermore, by studying the movement of the eigenvalues (also called *characteristic multipliers* for discrete-time systems) of the Jacobian under the variation of selected parameters, stability information

such as the occurrence of bifurcations and boundaries of operating regimes can be identified.

The Jacobian of the discrete-time map evaluated at the equilibrium point can be written as

$$J(\mathbf{X}_Q) = \frac{\partial \mathbf{f}}{\partial \mathbf{x}_n} - \frac{\partial \mathbf{f}}{\partial d_n}\left(\frac{\partial s}{\partial d_n}\right)^{-1}\left(\frac{\partial s}{\partial \mathbf{x}_n}\right)\Bigg|_{\mathbf{x}_n=\mathbf{X}_Q}. \quad (18)$$

Using (14) and (15), we can find all the derivatives in (18). First, $\partial \mathbf{f}/\partial \mathbf{x}_n$ can be found from (14), i.e.,

$$\frac{\partial \mathbf{f}}{\partial \mathbf{x}_n} = \mathbf{1} + T_s\left(d_n \mathbf{A}_1 + (1-d_n)\mathbf{A}_2\right). \quad (19)$$

Also, direct differentiation gives $\partial \mathbf{f}/\partial d_n$ as

$$\frac{\partial \mathbf{f}}{\partial d_n} = T_s(\mathbf{A}_1 - \mathbf{A}_2)\mathbf{x}_n + T_s(\mathbf{B}_1 - \mathbf{B}_2)E. \quad (20)$$

From (16), we obtain $\partial s/\partial \mathbf{x}_n$ readily as

$$\frac{\partial s}{\partial \mathbf{x}_n} = \mathbf{k} + \mathbf{k_1}\mathbf{A}_1 d_n T_s. \quad (21)$$

Again by direct differentiation, we get

$$\frac{\partial s}{\partial d_n} = T_s\left(\mathbf{k_1}\left(\mathbf{A}_1\mathbf{x}_n + \mathbf{B}_1 E\right) - (Mm_1 + m_c)\right). \quad (22)$$

Now, putting all the derivatives into (18) gives an expression for $J(\mathbf{X}_Q)$, as follows.

$$J(\mathbf{X}_Q) = \begin{bmatrix} J_{11} & J_{12} & J_{13} \\ J_{21} & J_{22} & J_{23} \\ J_{31} & J_{32} & J_{33} \end{bmatrix}. \quad (23)$$

Then, the eigenvalues can be obtained by solving the characteristic equation in λ

$$\det[\lambda \mathbf{1} - J(\mathbf{X}_Q)] = 0. \quad (24)$$

The expressions for J_{ij} in (23) and the solutions of (24) for the boost and buck converter systems can be found in Appendix II.

E. Eigenvalues of the Jacobian and Coexisting Bifurcations

Using the discrete-time model described in (14) and (15) and the Jacobian matrix (23), we can investigate the possible bifurcation behaviors exhibited by the period-1 orbits. Bifurcation and stability information can be obtained by examining the eigenvalues (characteristic multipliers) of the Jacobian derived in the foregoing. In particular, we are interested in the movement of the eigenvalues as some chosen parameters are varied. This information essentially reveals the bifurcation phenomena and the way in which variation of parameters affect the operation of the system. We will pay special attention to the movement of the eigenvalues as some chosen parameters are varied. Specifically, if all eigenvalues of the Jacobian are inside the unit circle, the equilibrium state about which the Jacobian has been evaluated is stable. Any crossing from the interior of the unit circle to the exterior indicates a loss of stability of the equilibrium state, i.e., a bifurcation occurs at the point of crossing [16]. The following judging criteria [14], based on the exact discrete-time model, are used here for identifying the system's bifurcation behavior:

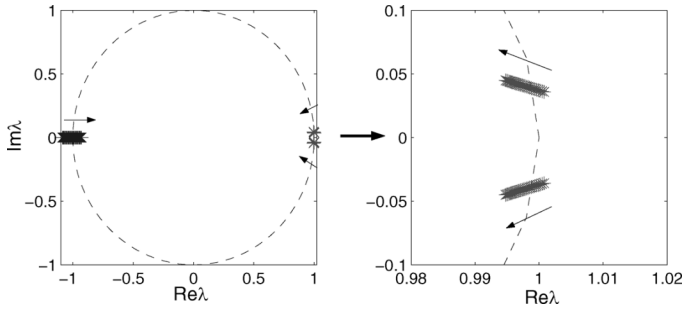

Fig. 7. Movement of eigenvalues for current-mode controlled boost converter. Left: loci of eigenvalues as E is varied for $L = 165\ \mu$H, $R = 30\ \Omega$, $\tau_a = 0.3196\ hboxms$ and $g = 1.0$. Right: close-up view of the complex pair of eigenvalues. Arrows indicate the direction of movement of the eigenvalues with E decreasing. As E is gradually increased, the complex pair of the eigenvalues move across the unit circle, indicating a slow-scale bifurcation, while the other eigenvalue is still outside the unit circle. These two conditions give coexisting bifurcation. Then, the real eigenvalue leaves the unit circle via –1, while the complex pair stays inside the unit cycle, indicating a period-doubling bifurcation.

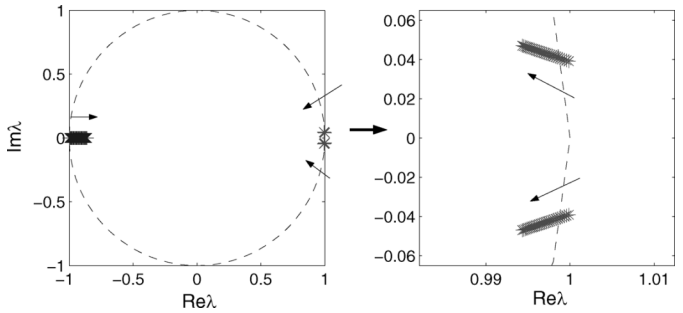

Fig. 8. Movement of eigenvalues for current-mode controlled boost converter. Left: loci of eigenvalues as E is varied for $L = 165\ \mu$H, $R = 25\ \Omega$, $\tau_a = 0.3196\ hboxms$ and $g = 1.0$. Right: close-up view of the complex pair of eigenvalues. Arrows indicate the direction of movement of the eigenvalues with E increasing. The real eigenvalue is always inside the unit circle, implying no possibility for fast-scale bifurcation. When the complex pair of eigenvalues leaves the unit circle as E is gradually increased, slow-scale bifurcation occurs.

1) Presence of all eigenvalues inside the unit circle indicates stable operation.
2) Slow-scale bifurcation occurs when a pair of complex conjugate eigenvalues move out of the unit circle while other eigenvalues stay inside the unit circle.
3) Fast-scale bifurcation occurs when a negative real eigenvalue moves out of the unit circle while all other eigenvalues stay inside the unit circle.
4) Coexisting fast-scale and slow-scale bifurcation occurs when a negative real eigenvalue and a pair of complex-conjugate eigenvalues move out of the unit circle at the same time.
5) Complex border collision bifurcation involving "saturated" operation occurs when some eigenvalues leap out of the unit circle.

The critical values of the bifurcation parameters are defined as those values where the locus of the eigenvalues crosses the unit circle. Using (23) and (24), we can generate loci of eigenvalues numerically. As we are interested in the loci of eigenvalues

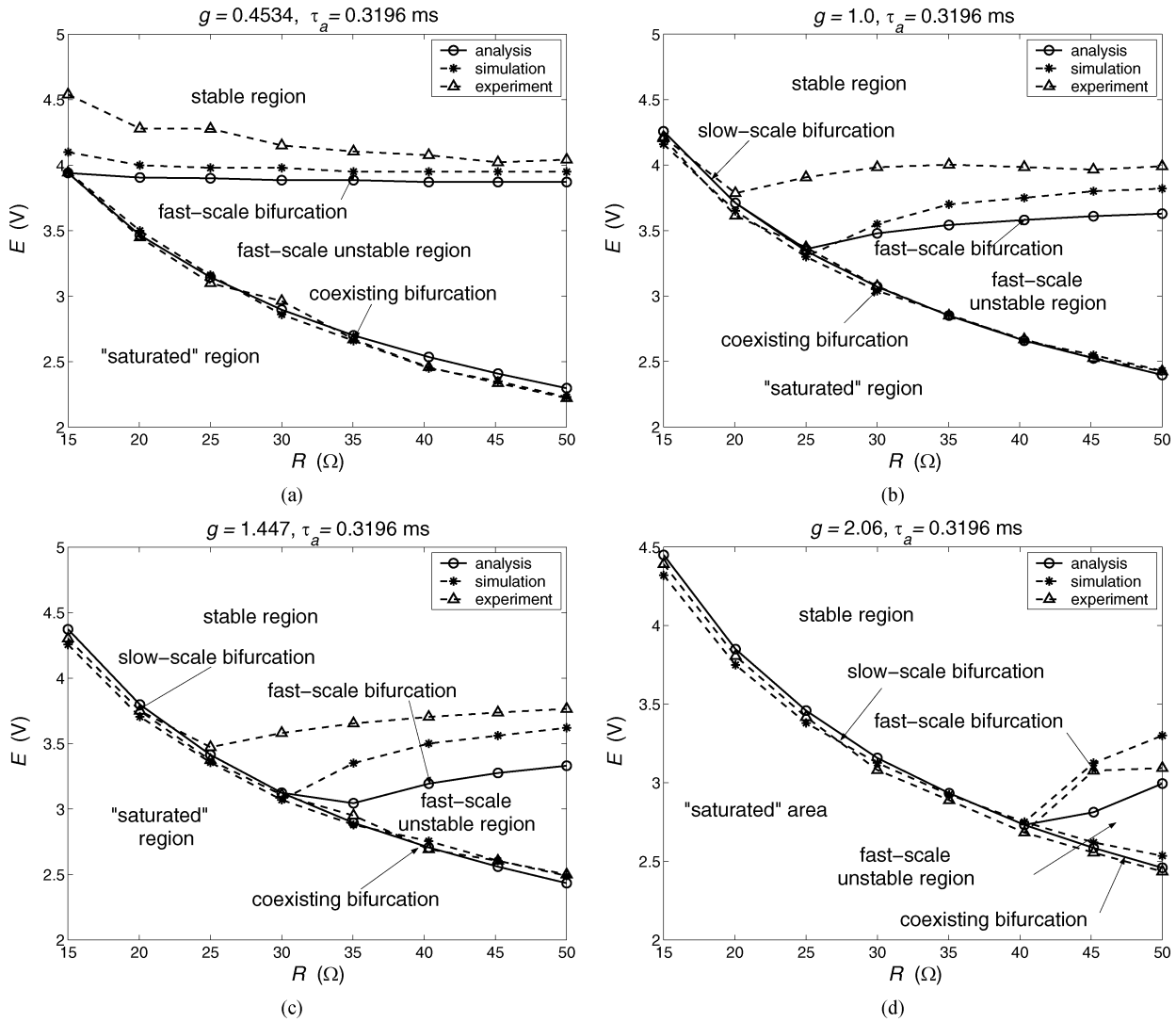

Fig. 9. Operating boundaries for the current-mode controlled boost converter plotted in the (R, E) parameter space, with $\tau_a = 0.3196\ hboxms$ and different values of feedback gain g.

when coexisting bifurcation occurs, the feedback gain and time constant are deliberately chosen to have a narrow bandwidth such that the system can become slow-scale unstable. We focus on the loci of varying input voltage E under different combinations of bifurcation parameters. The results with $L = 165\ \mu$H, $g = 1.0$ and $\tau_a = 0.3196$ ms for two different values of load resistance are shown in Tables II and III, and also illustrated in Figs. 7 and 8. It can be readily understood that the system's behavior can be identified according to the location of eigenvalues as described in the above judging criteria. We can see clearly that the crossing of complex eigenvalues with the unit circle means coexisting fast-scale and slow-scale bifurcation or slow-scale bifurcation depending upon whether the negative real eigenvalue is outside or inside the unit circle at the same time. This is consistent with the simulation and experimental results shown in Fig. 9. Similar loci of varying E with different R or τ_a can be obtained. They are omitted to save space here. Furthermore, the theoretical results will be shown in Section VI together with the simulation results to identify the boundaries of slow-scale bifurcation, fast-scale bifurcation and coexisting bifurcation.

As for the current-mode controlled buck and buck–boost converter systems, similar coexisting fast-scale and slow-scale bifurcation behavior has been observed, as shown in Section III, which can also be explained in terms of the movements of eigenvalues when some chosen parameters are varied.

VI. Application: Derivation of Boundaries of Operations

In this section, we will take a detailed look into the qualitative behavior of the system, and present the boundaries of stable region, slow-scale unstable region, fast-scale unstable region, and coexisting fast-scale and slow-scale unstable region in terms of selected circuit parameters. These operation boundaries, as shown in Figs. 9–11, are derived from cycle-by-cycle simulations, analytical solutions derived in Section V, as well as experimental measurements. The three kinds of results agree with each other. As mentioned previously, such boundaries of operation provide essential design-oriented information that allows the system parameters to be selected in an informed manner. Similar studies can be extended to other types of converters.

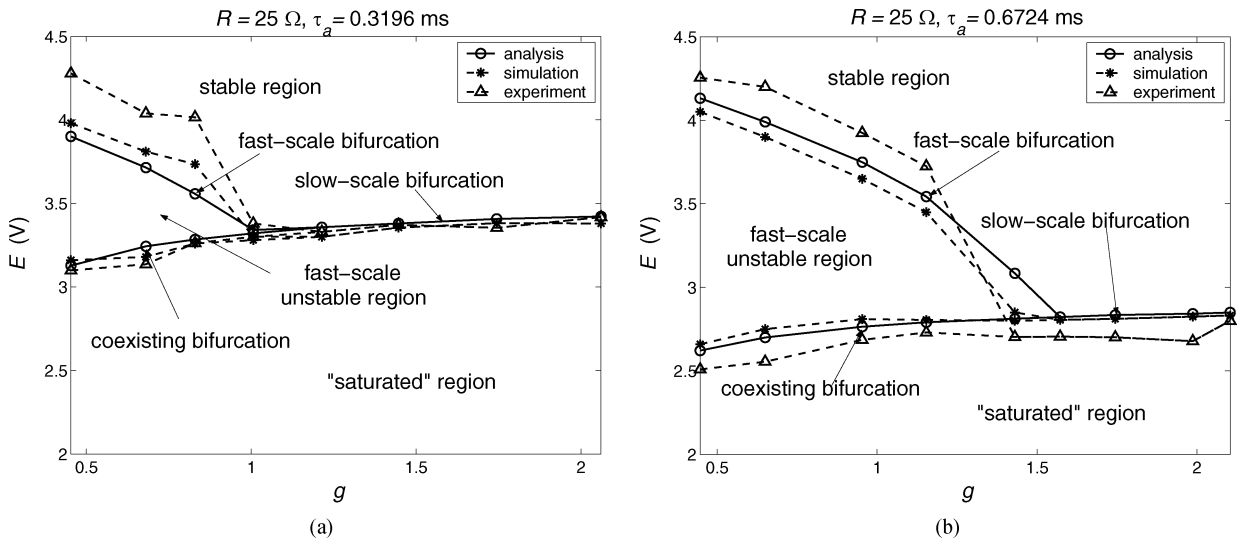

Fig. 10. Operating boundaries for the current-mode controlled boost converter plotted in the (g, E) parameter space, with $R = 25\ \Omega$ and different values of τ_a.

A. Effects of Varying Input Voltage and Load Resistance Under Fixed Feedback Time Constant

The behavior of the system varies with input voltage E and load R for a fixed relatively small value of time constant τ_a. Parameters except R, R_a, C_a and E are as listed in Table I. The operating boundaries in the parameter space of (R, E) with different values of feedback gain g under the same τ_a are shown in Fig. 9, where the boundaries divide regions of fast-scale unstable operation, stable operation, and "saturated" region. The transition from the "saturated" region to the fast-scale unstable region and the stable region are coexisting fast-scale and slow-scale bifurcation and slow-scale (Hopf type) bifurcation, respectively. Also, the transition from the stable region to the fast-scale unstable region is a period-doubling fast-scale bifurcation. From Fig. 9, we can see that coexisting bifurcation can easily occur at light load (i.e., load resistance has larger values), and the fast-scale region is reduced as g increases. We also observe that as E decreases, the system may leave the stable region via period-doubling (fast-scale) bifurcation, and finally goes into "saturated" operation via coexisting bifurcation. It may also go into "saturated" operation from the stable region directly via slow-scale bifurcation, depending upon the choice of the system's load and feedback gain.

B. Effects of Varying Input Voltage and Feedback Gain Under Varying Feedback Time Constant

The feedback gain g and time constant τ_a have obvious influences on the stability, especially for slow-scale bifurcation because of the bandwidth limitation imposed by the time constant. Here we study the behavior of the system when E and g are varied for different values of τ_a, and when E and τ_a are varied for different values of g. Parameters except R, R_a, C_a and E are kept as listed in Table I. The operating boundaries in the (g, E) parameter space with $R = 25\ \Omega$ for two different values of τ_a are shown in Fig. 10, from which we can see that coexisting bifurcation occurs for relatively smaller values of g, and that the fast-scale unstable region is enlarged when τ_a gets larger. However, further increase in τ_a (beyond about 0.7 ms) will have little effect on enlarging the fast-scale region as the input voltage range for coexisting or slow-scale bifurcation is bounded below by a minimum value. Obviously, on further decreasing τ_a, the parameter space of (g, E) contains only two regions, namely the stable region and the "saturated" region which are separated by a slow-scale bifurcation boundary.

Similar scenarios can be observed in the (τ_a, E) parameter space, as in Fig. 11. Here, we observe that for certain range of τ_a, varying g has a significant effect on the system's behavior, and specifically, coexisting bifurcation occurs for relatively small values of g. For larger values of g, the (τ_a, E) parameter space contains only the stable region and the "saturated" region which are separated by the slow-scale bifurcation boundary, as shown in Fig. 11(a).

C. General Observations

From the operation boundaries shown in Figs. 9–11, we may make the following general observations for the particular system under study. It should be emphasized that the above methodology for developing operation boundaries is design-oriented and can be used for any converter system.

1) Interacting bifurcation occurs easily for relatively large load resistance or small feedback gain.
2) Consistent with the usual understanding, the input voltage has significant effects on both the system's fast-scale and slow-scale stabilities. The fast-scale, slow-scale and coexisting fast-scale and slow-scale instabilities can be eliminated by increasing the input voltage.
3) Slow-scale or coexisting bifurcation can be eliminated by increasing the load resistance, which effectively changes the system's natural frequency.
4) The feedback gain can affect both fast-scale and slow-scale stabilities, in contrast to the usual belief that the feedback gain is related only to slow-scale stability.
5) For relatively small feedback gain, coexisting or slow-scale boundaries will shift toward small values of the input voltage. Increasing the feedback time constant enlarges the fast-scale bifurcation area, while the fast-scale boundary region is nearly unaffected for different values of the feedback time constant.

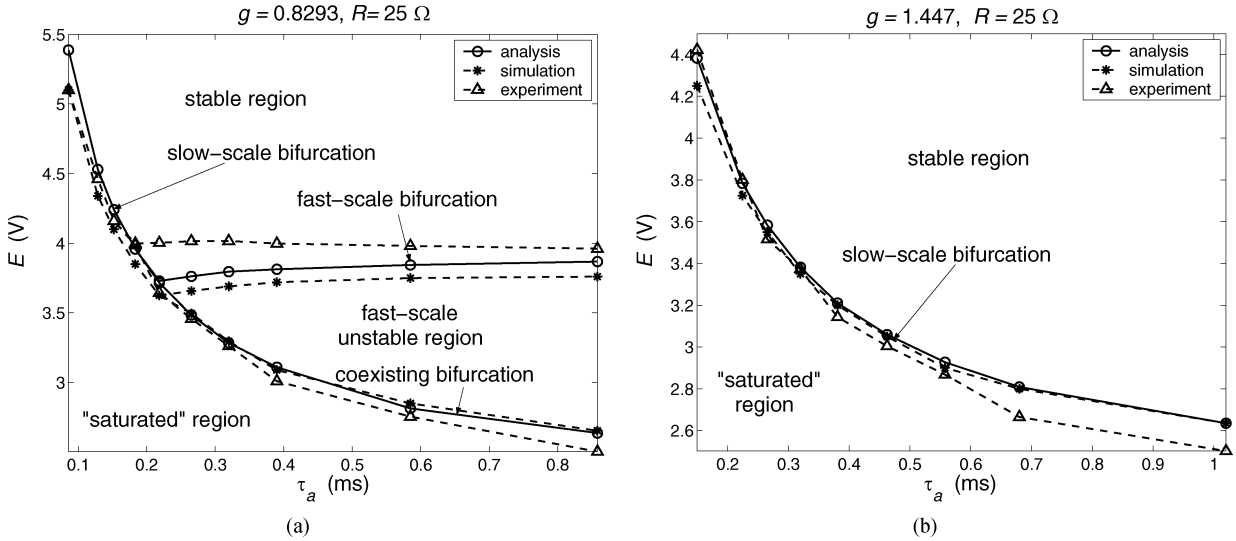

Fig. 11. Operating boundaries for the current-mode controlled boost converter plotted in the (τ_a, E) parameter space, with $R = 25\ \Omega$ and different values of g.

VII. Conclusion

In this paper, we have studied the coexistence of slow-scale and fast-scale bifurcations under variation of several important parameters. Our study has used "exact" cycle-by-cycle computer simulations, theoretical analysis based on a nonlinear discrete-time model, as well as experimental measurements. We have shown that current-mode controlled converters can lose stability via fast-scale instability, slow-scale instability, as well as interacting fast-scale and slow-sale instability. This finding clearly points out the mixing effect between the outer feedback loop and the inner current-programming loop which have been studied separately in many of the previous studies. Another important aspect of our study here is the gathering of operation boundaries in terms of practically relevant parameters, resulting in a useful form of information that can assist the design of practical converter systems, especially in avoiding or maintaining a particular kind of operation.

Appendix I

System matrices and fixed points for the current-mode controlled buck converter system are as follows.

$$\mathbf{A}_1 = \begin{bmatrix} -\frac{r_L+r_C+r_T}{L(1+k_c)} & -\frac{1}{L(1+k_c)} & 0 \\ \frac{1}{C(1+k_c)} & -\frac{1}{\tau_m(1+k_c)} & 0 \\ \frac{gr_c}{\tau_a(1+k_c)} & \frac{g}{\tau_a(1+k_c)} & 0 \end{bmatrix}, \tag{25}$$

$$\mathbf{A}_2 = \begin{bmatrix} -\frac{r_L+r_C+r_D}{L(1+k_c)} & -\frac{1}{L(1+k_c)} & 0 \\ \frac{1}{C(1+k_c)} & -\frac{1}{\tau_m(1+k_c)} & 0 \\ \frac{gr_c}{\tau_a(1+k_c)} & \frac{g}{\tau_a(1+k_c)} & 0 \end{bmatrix}, \tag{26}$$

$$\mathbf{B}_1 = \begin{bmatrix} \frac{1}{L} \\ 0 \\ -\frac{gk_dV_{\rm ref}}{\tau_a E} \end{bmatrix}, \ \mathbf{B}_2 = \begin{bmatrix} 0 \\ 0 \\ -\frac{gk_dV_{\rm ref}}{\tau_a E} \end{bmatrix}, \tag{27}$$

$$\begin{aligned} D_Q &= \frac{V_{00}\left[1+\frac{(r_D+r_L)}{R}\right]}{E-\frac{(r_T-r_D)V_{00}}{R}} \\ I_L &= \frac{V_{00}}{R} \\ V_A &= V_{\rm ref} - MI_L - (Mm_1+m_c)D_QT_s \end{aligned} \tag{28}$$

where $V_{00} = k_dV_{\rm ref}$ and $m_1 = (E - V_{00})/L$ is the rising slope of the inductor current.

System matrices and fixed points for current-mode controlled buck-boost converter system are as follows.

$$\mathbf{A}_1 = \begin{bmatrix} -\frac{r_L+r_T}{L} & 0 & 0 \\ 0 & -\frac{1}{\tau_m(1+k_c)} & 0 \\ 0 & \frac{g}{\tau_a(1+k_c)} & 0 \end{bmatrix}, \tag{29}$$

$$\mathbf{A}_2 = \begin{bmatrix} -\frac{r_L+r_D}{L} - \frac{r_C}{L(1+k_c)} & -\frac{1}{L(1+k_c)} & 0 \\ \frac{1}{C(1+k_c)} & -\frac{1}{\tau_m(1+k_c)} & 0 \\ \frac{gr_c}{\tau_a(1+k_c)} & \frac{g}{\tau_a(1+k_c)} & 0 \end{bmatrix}, \tag{30}$$

Here, $k_d = R_1/R_2$, and $g = R_a/(k_dR_3)$.

$$\mathbf{B}_1 = \begin{bmatrix} \frac{1}{L} \\ 0 \\ -\frac{gk_dV_{\rm ref}}{\tau_a E} \end{bmatrix}, \ \mathbf{B}_2 = \begin{bmatrix} 0 \\ 0 \\ -\frac{gk_dV_{\rm ref}}{\tau_a E} \end{bmatrix}, \tag{31}$$

$$\begin{aligned} V_{00} &= k_dV_{\rm ref} \\ D_Q &= 1 - \frac{b+\sqrt{b^2-4ac}}{2a} \\ I_L &= \frac{\frac{V_{00}}{R}}{1-D_Q} \\ V_A &= V_{\rm ref} - MI_L - \left(Mm_1 + m_c - \frac{gV_{00}}{\tau_m}\right)D_QT_s \end{aligned} \tag{32}$$

where $a = E + V_{00}/(1 + k_c)$, $b = -E - (r_T + r_D + r_C/(1 + kc))V_{00}/R$, $c = (r_T + r_L)V_{00}/R$, and $m_1 = E/L$ is the rising slope of the inductor current.

Appendix II

Expressions for the Jacobian matrix of the current-mode controlled boost converter described in Section V are summarized below. We set all parasitic resistances to zero for simplicity, i.e., $r_L = r_C = r_T = r_D = 0$. All the symbols are consistent with those given in the paper. For notational brevity,

we denote $m_e = M + m_c/m_1 - gk_dV_{\rm ref}/m_1\tau_m$, and $g_e = g\,(1 - D_QT_s/\tau_m + D_QT_s/\tau_a)$.

$$
\begin{aligned}
J_{11} &= 1 - \frac{M}{(1-D_Q)m_e} \\
J_{12} &= \frac{-(1-D_Q)T_s}{L} - \frac{g_e}{(1-D_Q)m_e} \\
J_{13} &= -\frac{1}{(1-D_Q)m_e} \\
J_{21} &= \frac{(1-D_Q)T_s}{C} + \frac{LM}{\tau_m(1-D_Q)^2m_e} \\
J_{22} &= 1 - \frac{T_s}{\tau_m} - \frac{Lg_e}{\tau_m(1-D_Q)^2m_e} \\
J_{23} &= \frac{L}{\tau_m(1-D_Q)^2m_e} \\
J_{31} &= 0, \quad J_{32} = \frac{gT_s}{\tau_a}, \quad J_{33} = 1.
\end{aligned}
$$

Upon expanding (24), we get the following characteristic polynomial equation:

$$a_0\lambda^3 + a_1\lambda^2 + a_2\lambda + a_3 = 0 \tag{33}$$

where

$$
\begin{aligned}
a_0 &= 1 \\
a_1 &= -(J_{11} + J_{22} + J_{33}) \\
a_2 &= J_{11}J_{22} + J_{11}J_{33} + J_{22}J_{33} - J_{21}J_{22} - J_{23}J_{32} \\
a_3 &= -J_{11}J_{22}J_{33} - J_{13}J_{21}J_{32} + J_{11}J_{23}J_{32} + J_{33}J_{12}J_{21}.
\end{aligned}
$$

The solutions of (33) are:

$$
\begin{aligned}
\lambda_1 &= u + v - \frac{1}{3}a_1 \\
\lambda_2 &= -\frac{1}{2}(u+v) - \frac{1}{3}a_1 + \frac{\sqrt{3}}{2}(u-v)j \\
\lambda_3 &= -\frac{1}{2}(u+v) - \frac{1}{3}a_1 - \frac{\sqrt{3}}{2}(u-v)j
\end{aligned} \tag{34}
$$

where

$$
\begin{aligned}
p &= a_2 - \frac{1}{3}a_1^2 \\
q &= \frac{2}{27}a_1^3 - \frac{1}{3}a_1a_2 + a_3 \\
h &= \left(\frac{q}{2}\right)^2 + \left(\frac{p}{3}\right)^3 \\
u &= \sqrt[3]{-\left(\frac{q}{2}\right) + \sqrt{h}} \\
v &= \sqrt[3]{-\left(\frac{q}{2}\right) - \sqrt{h}}.
\end{aligned}
$$

REFERENCES

[1] R. Redl and N. O. Sokal, "Current-mode control, five different types, used with three basic classes of power converters," in *IEEE Power Electron. Specialists Conf. Rec.*, 1985, pp. 771–775.

[2] C. K. Tse, *Complex Behavior of Switching Power Converters*. Boca Raton, FL: CRC Press, 2003.

[3] S. Banerjee and G. Verghese, Eds., Nonlinear phenomena in power electronics: attractors, bifurcations, chaos and nonlinear control New York, IEEE Press, 2000.

[4] S. Banerjee and K. Chakrabarty, "Nonlinear modeling and bifurcations in the boost converter," *IEEE Trans. Power Electron.*, vol. 13, no. 2, pp. 252–260, Apr. 1988.

[5] W. C. Y. Chan and C. K. Tse, "Study of bifurcations in current-programmed dc/dc boost converters: From quasi-periodicity to period-doubling," *IEEE Trans. Circuits Syst. I, Fundam. Theory Appl.*, vol. 44, no. 12, pp. 1129–1142, Dec. 1997.

[6] A. El Aroudi, L. Benadero, E. Toribio, and G. Oliver, "Hopf bifurcation and chaos from torus breakdown in a PWM voltage-controlled dc-dc boost converter," *IEEE Trans. Circuits Syst. I, Fundam. Theory Appl.*, vol. 46, no. 11, pp. 1374–1382, Nov. 1999.

[7] C. K. Tse, Y. M. Lai, and H. H. C. Iu, "Hopf bifurcation and chaos in a free-running current-controlled Ćuk switching regulator," *IEEE Trans. Circuits Syst. I, Fundam. Theory Appl.*, vol. 47, no. 4, pp. 448–457, Apr. 2000.

[8] S. C. Wong, C. K. Tse, M. Orabi, and T. Ninomiya, "The method of double averaging: An approach for modeling power-factor-correction power converters," *IEEE Trans. Circuits Syst. I, Reg. Papers*, vol. 53, no. 2, pp. 454–462, Feb. 2006.

[9] H. H. C. Iu and C. K. Tse, "Study of low-frequency bifurcation of a parallel-connected boost converter system via averaged models," *IEEE Trans. Circuits Syst. I, Fundam. Theory Appl.*, vol. 50, no. 5, pp. 679–686, May 2003.

[10] S. C. Wong, C. K. Tse, and K. C. Tam, "Intermittent chaotic operation in switching power converters," *Int. J. Bifurc. Chaos*, vol. 14, no. 8, pp. 1971–2978, Aug. 2004.

[11] H. H. C. Iu, Y. Zhou, and C. K. Tse, "Fast-scale instability in a PFC boost converter under average current-mode control," *Int. J. Circuit Theory Appl.*, vol. 31, no. 6, pp. 611–624, Nov.-Dec. 2003.

[12] X. Wu, C. K. Tse, O. Dranga, and J. Lu, "Fast-scale instability of single-stage power-factor-correction power supplies," *IEEE Trans. Circuits Syst. I, Reg. Papers*, vol. 53, no. 1, pp. 204–213, Jan. 2006.

[13] S. K. Mazumder, A. H. Nayfeh, and D. Boroyevich, "Theoretical and expenrimental investigation of the fast-scale and slow-scale instabilities of a dc-dc converter," *IEEE Trans. Power Electron.,*, vol. 16, no. 2, pp. 201–216, Apr. 2001.

[14] Y. Chen, C. K. Tse, and S.-S. Qiu, "Interaction of fast-scale and slow-scale bifurcations in current-mode controlled dc/dc converters," in *Int. Symp. Nonlinear Theory and Its Appl. , (NOLTA'06)*, Bologna, Italy, Sep. 2006, pp. 175–179.

[15] A. V. Anunciada and M. M. Silva, "On the stability and subharmonic susceptiblity of current-mode controlled converters," in *IEEE Power Electron. Specialists Conf. Rec.*, 1992, pp. 345–353.

[16] S. Pavljasevic and D. Maksimovic, "Using a discrete-time model for large-signal analysis of a current-programmed boost converter," in *IEEE Power Electron. Specialists Conf. Rec.*, 1991, pp. 715–721.

[17] J. Guckenheimer and P. Holmes, *Nonlinear Oscillations in Dynamical Systems and Bifurcations of Vector Fields*. New York: Springer-Verlag, 1983.

[18] B. Robert and A. El Araudi, "Discrete time model of a multi-cell dc/dc converter: Nonlinear approach," *Int. J. Math. Computers in Simulations*, vol. 71, no. 4–6, pp. 310–319, May 2006.

[19] T. S. Parker and L. O. Chua, *Practical Numerical Algorithms for Chaotic Systems*. New York: Springer-Verlag, 1989.

Yanfeng Chen received the B.E. degree in electromagnetic measurement technology and instruments from China Jiliang University, China, in 1992, the M.E. degree in power electronics technology from Wuhan University, Hubei, China, in 1995, and the Ph.D. degree in circuits and systems from South China University of Technology, Guangzhou, China, in 2000.

She was a Postdoctoral Fellow from August 2000 to December 2002 with the Department of Electronics Engineering, Sun Yat Sen University, Guangzhou, China, working on nonlinear circuits and hot-swap technology for telecom products. From November 2005 to December 2006, she was a Research Associate with the Department of Electronic and Information Engineering, Hong Kong Polytechnic University, Hong Kong. Since January 2003, she has been an Associate Professor with the School of Electronic and Information Engineering, South China University of Technology, China. Her main research interests include modeling and analysis of nonlinear systems and power electronics.

Chi K. Tse (M'90–SM'97–F'06) received the BEng (Hons) degree with first class honors in electrical engineering and the Ph.D. degree from the University of Melbourne, Australia, in 1987 and 1991, respectively.

He is presently Chair Professor and Head of Department of Electronic and Information Engineering, Hong Kong Polytechnic University, Hong Kong. He is a Guest Professor of Wuhan University, China, and Southwest University, China. His research interests include power electronics, complex networks and nonlinear systems.

He is the author of *Linear Circuit Analysis* (London, U.K.: Addison-Wesley 1998) and *Complex Behavior of Switching Power Converters* (Boca Raton: CRC Press, 2003), coauthor of *Chaos-Based Digital Communication Systems*(Heidelberg, Germany: Springer-Verlag, 2003) and *Chaotic Signal Reconstruction with Applications to Chaos-Based Communications* (Beijing: TUP, 2005), and co-holder of a US patent and two pending patents. In 1987, he was awarded the L.R. East Prize by the Institution of Engineers, Australia, the IEEE TRANSACTIONS ON POWER ELECTRONICS Prize Paper Award in 2001, and the International Journal of Circuit Theory and Applications Best Paper Award in 2003. In 2007, he was awarded the Distinguished International Research Fellowship by the University of Calgary, Canada. While with the Hong Kong Polytechnic University, he received twice the President's Award for Achievement in Research, the Faculty's Best Researcher Award, the Research Grant Achievement Award and a few other teaching awards.

From 1999 to 2001, he served as an associate editor for the IEEE IEEE TRANSACTIONS ON CIRCUITS AND SYSTEMS—I: FUNDAMENTAL THEORY AND APPLICATIONS, and since 1999 he has been an associate editor for the IEEE TRANSACTIONS ON POWER ELECTRONICS. In 2005, he served as an IEEE Distinguished Lecturer. Presently he also serves as the Editor-in-Chief of the IEEE Circuits and Systems Society Newsletter, Associate Editor for the International Journal of Systems Science, IEEE Circuits and Systems Magazine and the International Journal of Circuit Theory and Applications, and Guest Editor of a few other journals.

Shui-Sheng Qiu was born in Guangdong, China, in 1939. He received the M.Sc. degree in electrical engineering and the Ph.D. degree in nonlinear oscillation theory, both from the South China University of Technology, Guangzhou, China, in 1963 and 1966, respectively.

From 1967 to 1968, he was with the South China University of Technology, China. From 1970 to 1978, he worked for Shaokuan Radio Company, Guangdong, China. Since 1978, he has been on the staff of the South China University of Technology, Guangzhou, and is currently a Professor in the School of Electronics and Information Engineering. From 1984 to 1986, and 1990 to 1991, respectively, he was a visiting professor at the University of Alberta, Edmonton, Canada. In 1990, was a visiting professor at the Portland State University, Portland, USA, and in 2001, was a visiting professor at the Hong Kong Polytechnic University, Hong Kong, China. He proposed the principle of the equivalent small parameter method in 1985. He is the author of the book *Nonlinear Circuits and Systems* (Univ. EST Press, 1990) and over 80 technical papers. His current research interests are in the areas of nonlinear circuits and systems, power electronics, chaos and secure communication. He is the Chairman of the Committee of Nonlinear Circuits and Systems of the Chinese Institute of the Electronics, China, and is a member of the Editorial Committee of the *Journal of Electronics,* China.

Lars Lindenmüller is currently working toward the Dipl.-Ing. (M.Sc.) degree in electrical engineering at the Faculty of Electrical Engineering and Information Technology, Technische Universität Dresden, Germany.

From September 2006 to August 2007, he was an exchange student with the Hong Kong Polytechnic University and worked in the Applied Nonlinear Circuits and Systems Research Group. His research interests include renewable energy sources, power electronics and drives.

Wolfgang Schwarz (M'92) received the Dipl.-Ing. (M.S.), Dr.-Ing. (Ph.D.) and Dr.-Ing. habil. degrees from the Technical University Dresden (TUD), Dresden, Germany, in 1965, 1969, and 1976, respectively.

He has been a Research Assistant and Lecturer at TUD from 1965 to 1969, an Assistant Professor for Control Engineering from 1969 to 1974. He was a Full Professor for Information Technology at the University of Applied Sciences, Mittweida, Germany, from 1969 to 1983. From 1983 to 1992, he was a Full Professor for Electronic Circuits at TUD. Since 1992, he has been University Professor at TUD for Fundamentals of Electrical Engineering and teaches basic courses in electrical engineering and advanced courses on electronic circuits and nonlinear circuits. His research interests include nonlinear dynamic circuits, dynamical chaos and statistical analysis, and design of nonlinear circuits and systems. He was an invited professor at the Moscow Technical University for Communication and Informatics, Moscow, U.S.S.R., in 1974 and 1977, invited researcher at the University of California, Berkeley, CA, in 1991 and invited professor at Waseda University, Tokyo, Japan, in 2001. In 2008, he is a visiting professor at the Hong Kong Polytechnic University.